

## Enhanced Thermoelectric Power Factor of Tensile Drawn Poly(3-hexylthiophene)

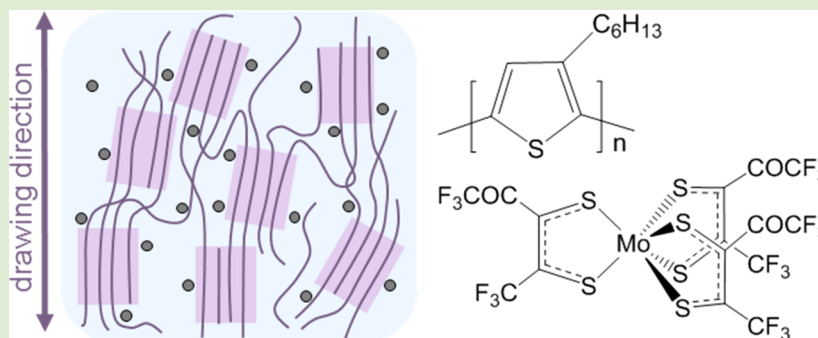
Jonna Hynynen,<sup>†</sup> Emmy Järsvall,<sup>†</sup> Renee Kroon,<sup>†</sup> Yadong Zhang,<sup>‡</sup> Stephen Barlow,<sup>‡</sup> Seth R. Marder,<sup>‡</sup> Martijn Kemerink,<sup>§</sup> Anja Lund,<sup>†</sup> and Christian Müller<sup>\*,†</sup>

<sup>†</sup>Department of Chemistry and Chemical Engineering, Chalmers University of Technology, 41296 Göteborg, Sweden

<sup>‡</sup>School of Chemistry and Biochemistry and Center for Organic Photonics and Electronics, Georgia Institute of Technology, Atlanta, Georgia 30332-0400, United States

<sup>§</sup>Complex Materials and Devices, Department of Physics, Chemistry and Biology (IFM), Linköping University, SE-581 83 Linköping, Sweden

### S Supporting Information



**ABSTRACT:** The thermoelectric power factor of a broad range of organic semiconductors scales with their electrical conductivity according to a widely obeyed power law, and therefore, strategies that permit this empirical trend to be surpassed are highly sought after. Here, tensile drawing of the conjugated polymer poly(3-hexylthiophene) (P3HT) is employed to create free-standing films with a high degree of uniaxial alignment. Along the direction of orientation, sequential doping with a molybdenum tris(dithiolene) complex leads to a 5-fold enhancement of the power factor beyond the predicted value, reaching up to  $16 \mu\text{W m}^{-1} \text{K}^{-2}$  for a conductivity of about  $13 \text{ S cm}^{-1}$ . Neither stretching nor doping affect the glass transition temperature of P3HT, giving rise to robust free-standing materials that are of interest for the design of flexible thermoelectric devices.

Conjugated polymers are heralded as materials that combine excellent electronic and mechanical properties. However, most current progress has focused on printed architectures where the polymer is typically deposited as a thin layer on a carrier substrate. Instead, mechanically robust and free-standing bulk materials are needed for a number of emerging applications such as textile electronics<sup>1</sup> and organic thermoelectrics,<sup>2,3</sup> where up to a millimeter-thick structures must be used to maintain heat gradients. When doping is required, a necessary compromise between the electrical and the mechanical properties arises. With regard to thermoelectrics, doping introduces charge carriers, which increases the conductivity  $\sigma$  and decreases the Seebeck coefficient  $\alpha$ , resulting in a power factor  $\alpha^2\sigma$  that typically scales with  $\sigma$  according to an empirical power law:<sup>4</sup>

$$\alpha^2\sigma \propto \sigma^{1/2} \quad (1)$$

An important factor to consider that may not be fully appreciated is that the introduction of dopant molecules (or ions) can reduce the mechanical coupling between polymer chains.<sup>1</sup> Accordingly, at high dopant concentrations, the

electronic coupling suffers, which is typically referred to as “perturbations of the morphology”.<sup>5</sup> Further, it is feasible that a stiffening of polymer chains due to the presence of (dopant-induced) polarons could increase the glass transition temperature  $T_g$ , leading to a more brittle material.

One powerful tool to enhance both the mechanical and the electrical properties is solid-state drawing, which can be carried out on films and is an essential step in many fiber spinning processes.<sup>1</sup> Early studies of stretch-aligned conjugated polymers, including polyacetylene,<sup>6</sup> polyaniline,<sup>7</sup> polyphenylenevinylenes (PPVs),<sup>8–10</sup> and polythiophenes<sup>11–13</sup> have found that chain orientation results in a considerable increase in electrical conductivity along the drawing direction. The influence of solid-state drawing on the Seebeck coefficient is less clear; upon stretching,  $\alpha$  has been reported to decrease in the case of I<sub>2</sub>-

**Received:** October 24, 2018

**Accepted:** December 19, 2018

**Published:** December 26, 2018

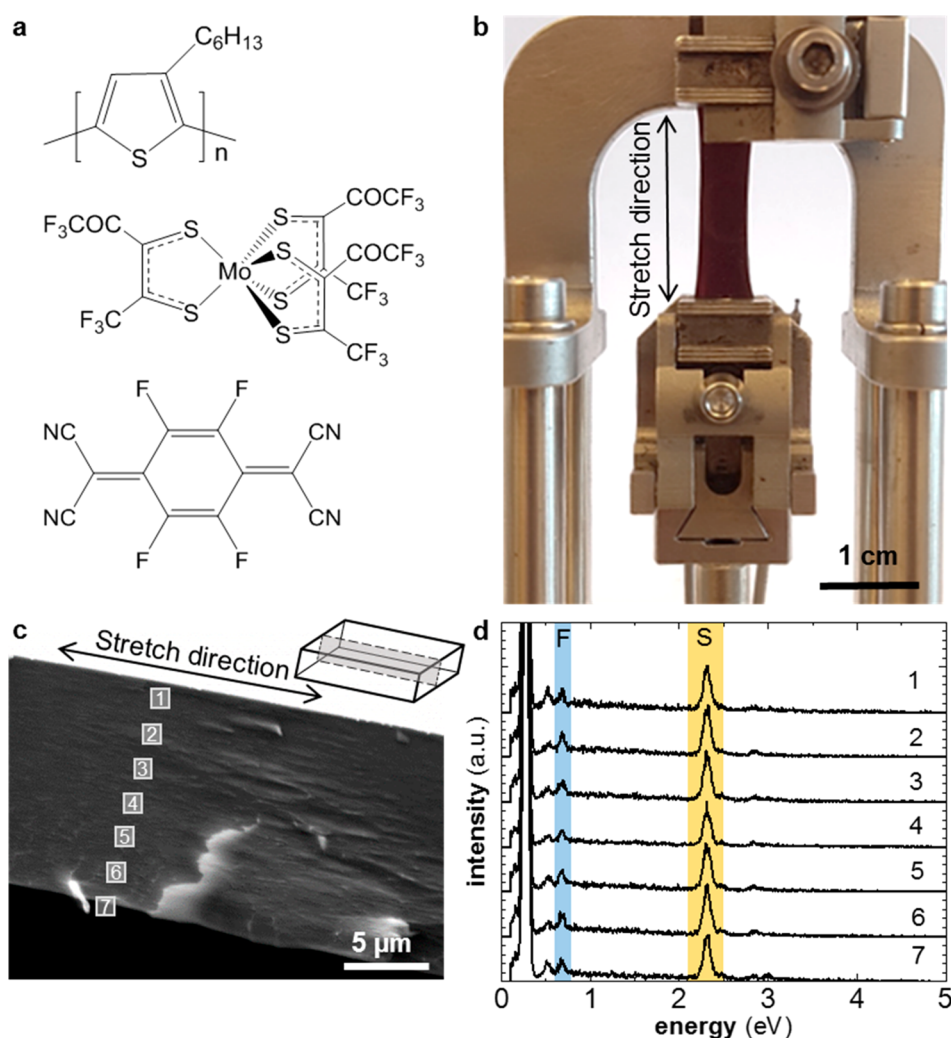


**Figure 1.** (a) Chemical structures of P3HT, Mo(tfd-COCF<sub>3</sub>)<sub>3</sub>, and F4TCNQ. (b) Stretched film of P3HT, clamped in a DMA instrument. (c) Scanning electron microscopy (SEM) image of the freeze-fractured surface used for energy dispersive X-ray spectroscopy (EDX); inset: sketch of EDX sample, the freeze fractured surface is shown by the dashed line. (d) EDX spectrogram of stretched P3HT sequentially doped with Mo(tfd-COCF<sub>3</sub>)<sub>3</sub> for 72 h; fluorine and sulfur peaks are colored blue and yellow, respectively (note that the molybdenum and sulfur peaks overlap).

doped and FeCl<sub>3</sub>-doped polyacetylene<sup>14</sup> and to not change along the drawing direction in the case of I<sub>2</sub>-doped PPVs<sup>8</sup> and polyaniline doped with oxalic acid,<sup>15</sup> but to increase in the case of polyaniline doped with camphorsulfonic acid.<sup>16</sup> Hence, it is currently not evident how tensile deformation will influence the thermoelectric properties of bulk materials. In contrast, for thin films of polythiophenes, a number of recent reports have indicated that in-plane anisotropy can enhance the power factor beyond the trend predicted by eq 1,<sup>5,17</sup> which most (less oriented) organic semiconductors appear to obey.<sup>4</sup> For instance, Hamidi-Sakr et al. have studied 40 nm thin films of poly(3-hexylthiophene), aligned by rubbing and subsequently doped with 2,3,5,6-tetrafluoro-7,7,8,8-tetracyanoquinodimethane (F4TCNQ).<sup>17</sup> An up to 2-fold increase in the Seebeck coefficient and up to 4-fold increase in electrical conductivity along the rubbing direction gave rise to a power factor of 8.5 μW m<sup>-1</sup> K<sup>-2</sup>. Hence, we set out to investigate if structural anisotropy is a suitable strategy to enhance the power factor of bulk materials beyond values predicted by the empirical power law and how this relates to the mechanical properties of the materials.

In this study, we carry out a systematic comparison of free-standing P3HT films, which we orient through solid-state tensile drawing. We correlate the mechanical and electrical properties of isotropic and stretch-aligned samples, both parallel and perpendicular to the drawing direction. We primarily use the molybdenum tris(dithiolene) complex Mo(tfd-COCF<sub>3</sub>)<sub>3</sub> (see Figure 1 for chemical structure), which is able to diffuse into P3HT thin films,<sup>18</sup> and also include F4TCNQ in our study for comparison. We find that along the alignment direction the power factor can be increased by up to five times beyond the value predicted by eq 1, whereas *T<sub>g</sub>* is unaffected, which opens up the possibility to use free-standing materials for the design of flexible thermoelectric devices.

We chose to work with a high molecular weight batch of P3HT (number-average molecular weight of *M<sub>n</sub>* ~ 91 kg mol<sup>-1</sup>; polydispersity index ~ 1.8, regioregularity ~ 93%) that is able to form tie chains,<sup>19</sup> which we expect to ease solid-state drawing. Films with a thickness of 10–40 μm were cast from 80 °C hot concentrated (20 g L<sup>-1</sup>) *p*-xylene solutions onto 90 °C hot glass substrates to produce smooth films. Dried films were then peeled from the substrate and tensile drawn at 60 °C and a rate of 0.5 mm min<sup>-1</sup> using a dynamic mechanical analysis (DMA)

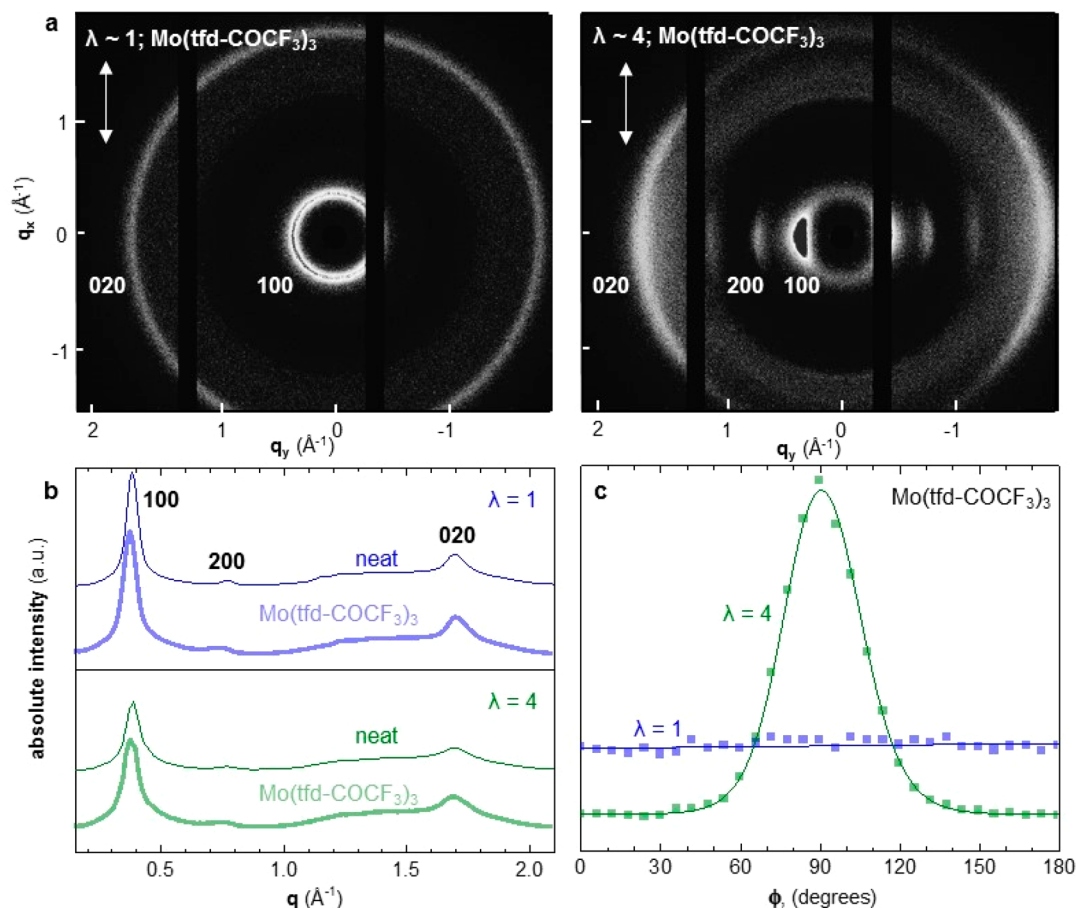


**Figure 2.** (a) Wide angle X-ray scattering (WAXS) patterns of as-cast ( $\lambda = 1$ ) and tensile drawn P3HT ( $\lambda \sim 4$ ; arrows indicate drawing direction) sequentially doped with  $\text{Mo}(\text{tfd-COCF}_3)_3$ . (b) Diffractograms showing the radial intensity distribution for  $\lambda = 1$  (blue) and  $\lambda \sim 4$  (green). (c) Angular distribution of the prominent 100 diffraction (azimuthal angle  $\phi = 0, \pi$  is parallel to drawing direction).

instrument to prepare samples for further analysis (cf. Figure 1b). The stretching was terminated when a draw ratio of  $\lambda \sim 4$  had been reached. The maximum draw ratio beyond which fracture occurred was  $\lambda_{\text{max}} \sim 5$ .

We used wide-angle X-ray scattering (WAXS) to compare the degree of anisotropy of as-cast and stretched samples (Figure 2). X-ray diffractograms of as-cast P3HT indicate an isotropic distribution of crystallites. For the stretched films we deduce considerable orientation of ordered domains, with alignment of the polymer backbone along the fiber axis, as evidenced by the strong equatorial 100 and 020 diffraction peaks. Angular integration of the 100 diffraction peak was used to calculate Herman's orientation factor,  $f$ :

$$f = \frac{1}{2}(3\langle \cos^2 \phi \rangle - 1) = \frac{\int_0^\pi \frac{1}{2}(3 \cos^2 \phi - 1)I(\phi) \sin \phi d\phi}{\int_0^\pi I(\phi) \sin \phi d\phi} \quad (2)$$

where  $\phi$  is the angle of orientation with respect to the direction of tensile drawing ( $\phi = 0, \pi$  is parallel to drawing direction) and  $I(\phi)$  is the radially integrated intensity of the 100 diffraction peak. The Herman's orientation factor changed from  $f \sim 0$  to  $-0.3$  upon stretching, which is indicative of a substantial degree of alignment. First heating differential scanning calorimetry (DSC) thermograms of as-cast and tensile-drawn material show the same melting temperature  $T_m \sim 239^\circ\text{C}$ , but a slight increase of the enthalpy of fusion from  $\Delta H_f \sim 17 \text{ J g}^{-1}$  to  $21 \text{ J g}^{-1}$  (Supporting Information, Figure S1), which suggests the same crystal size but somewhat higher crystallinity of drawn P3HT.

Sequential doping allowed us to introduce the dopant subsequent to film casting and solid-state drawing. Films of P3HT were immersed for 48 to 72 h in solutions of the dopant  $\text{Mo}(\text{tfd-COCF}_3)_3$  or F4TCNQ in acetonitrile (AcN;  $5 \text{ g L}^{-1}$ ), an orthogonal solvent in which P3HT is insoluble. Both as-cast and stretched films show an increase in weight by  $\sim 30 \text{ wt } \%$  upon doping with  $\text{Mo}(\text{tfd-COCF}_3)_3$ , and by  $\sim 6 \text{ wt } \%$  in case of F4TCNQ, indicating a dopant concentration of  $\sim 9$  and  $\sim 4 \text{ mol } \%$ , respectively (note that an increase in dopant concentration to  $15 \text{ g L}^{-1}$  resulted in similar concentrations of  $\sim 9$  and  $\sim 5 \text{ mol } \%$ ). We carried out energy dispersive X-ray spectroscopy (EDX) on doped films to investigate to which extent the larger dopant  $\text{Mo}(\text{tfd-COCF}_3)_3$  had diffused into the sample (Figure 1 and Supporting Information, Figure S2). EDX of cross sections of both as-cast and stretched films indicates that both dopants are evenly distributed throughout the bulk of the sample, as evidenced by a constant ratio of the intensity of the sulfur and fluorine signals, and a similar strength of the latter (cf. EDX of P3HT doped with F4TCNQ, Supporting Information, Figure S3). We conclude that sequential doping for the period of time chosen here, that is, 72 h, is sufficient to saturate the P3HT films with dopant.

To investigate the position of the dopant within the solid-state nanostructure, we compared WAXS diffractograms of as-cast and doped films.  $\text{Mo}(\text{tfd-COCF}_3)_3$  doped films only show a marginal change in the  $q$ -spacing of crystalline peaks in comparison to the neat film of P3HT (Figure 2), which suggests

that the bulky  $\text{Mo}(\text{tfd-COCF}_3)_3$  does not penetrate the crystallites but resides in the amorphous domains. In contrast, WAXS diffractograms of F4TCNQ doped films (as-cast and stretched) confirm that the dopant ingresses into crystalline domains and sits between the side chains, as evidenced by the previously reported shift in the 100 and 020 diffraction peaks (Supporting Information, Figure S4).<sup>20–23</sup> Further, we confirm that doping with  $\text{Mo}(\text{tfd-COCF}_3)_3$  does not change the degree of anisotropy obtained through solid state drawing (cf. Supporting Information, Table S1).

Doping can have a pronounced effect on the mechanical properties of a conjugated polymer.<sup>1</sup> We therefore recorded the storage modulus  $E'$  and loss modulus  $E''$  from  $-100$  to  $+40$  °C using variable-temperature DMA (Figure 3 and Supporting Information, Figures S5 and S6). We observe a  $T_g \sim 20$  °C that does not change upon tensile drawing or doping with  $\text{Mo}(\text{tfd-COCF}_3)_3$  (Table 1), which implies that this type of dopant does not result in a more brittle material. Instead, doping with F4TCNQ appears to slightly increase the  $T_g$  to 40 °C (Supporting Information, Figure S6). Further, both neat and  $\text{Mo}(\text{tfd-COCF}_3)_3$ -doped P3HT feature a pronounced  $T_\beta \sim -90$  °C, below which side chain relaxation becomes arrested,<sup>24</sup> meaning that the polymer should be characterized by a high impact toughness. As-cast P3HT features a storage modulus of  $E' \sim 0.6$  GPa at 0 °C, which increases to  $E_{\parallel}' \sim 1.1$  GPa upon tensile drawing when measured parallel to the direction of orientation (Table 1). Instead, the perpendicular storage modulus  $E_{\perp}'$  decreases to 0.2 GPa, giving rise to a high anisotropy of  $E_{\parallel}'/E_{\perp}' \sim 6$ . Upon doping the storage modulus of as-cast samples only slightly decreases to  $E' \sim 0.5$  GPa. For stretched samples we measure the same  $E_{\perp}'$  before and after doping, but observe a 3-fold decrease in storage modulus parallel to the direction of orientation to  $E_{\parallel}' \sim 0.4$  GPa, leading to a lower anisotropy of about  $E_{\parallel}'/E_{\perp}' \sim 4$ . We explain the change in storage modulus upon doping with a reduced cohesion between adjacent polymer chains in amorphous domains where the  $\text{Mo}(\text{tfd-COCF}_3)_3$  dopant is located, that is, the dopant acts as a plasticizer (note that deformation was carried out in the elastic region where only amorphous domains deform). Nevertheless, an appreciable storage modulus is maintained, for example, the value  $E_{\parallel}' \sim 0.2$  GPa at room temperature is similar to the modulus of unoriented low-density polyethylene (LDPE).<sup>25</sup>

In a further set of experiments, we explored the thermoelectric properties of  $\text{Mo}(\text{tfd-COCF}_3)_3$ -doped P3HT. For as-cast films we measure a conductivity of  $\sigma_0 \sim 0.3 \pm 0.1$  S  $\text{cm}^{-1}$  and a Seebeck coefficient of  $\alpha_0 \sim 138 \pm 1$   $\mu\text{V K}^{-1}$ , which differ considerably from the corresponding values of  $34.1 \pm 0.2$  S  $\text{cm}^{-1}$  and  $64 \pm 1$   $\mu\text{V K}^{-1}$ , respectively, found for 70 nm thin films. It appears that the bulk samples studied here are less heavily doped than thin spin-coated films. Since we do not observe a gradient in dopant concentration (cf. EDX; Figure 1), we argue that our bulk samples are saturated with the  $\text{Mo}(\text{tfd-COCF}_3)_3$  dopant, and therefore, thin films cannot merely contain a higher concentration of the dopant. We tentatively propose that the higher conductivity of thin films is due to a more strongly doped surface layer where additional dopant does not need to fully diffuse into the polymer to still dope a significant fraction of the active layer. Further, we would like to point out that  $\text{Mo}(\text{tfd-COCF}_3)_3$  (electron affinity  $EA \sim 5.6$  eV;<sup>26,27</sup> reduction potential  $E_{\text{red}} \sim +0.39$  V vs ferrocene<sup>28</sup>) is a stronger oxidant than F4TCNQ ( $EA \sim 5.2$  eV<sup>29</sup>), which allows the former, but not the latter, to dope disordered P3HT (cf. doping of regiorandom P3HT; Supporting Information, Figure S7). This

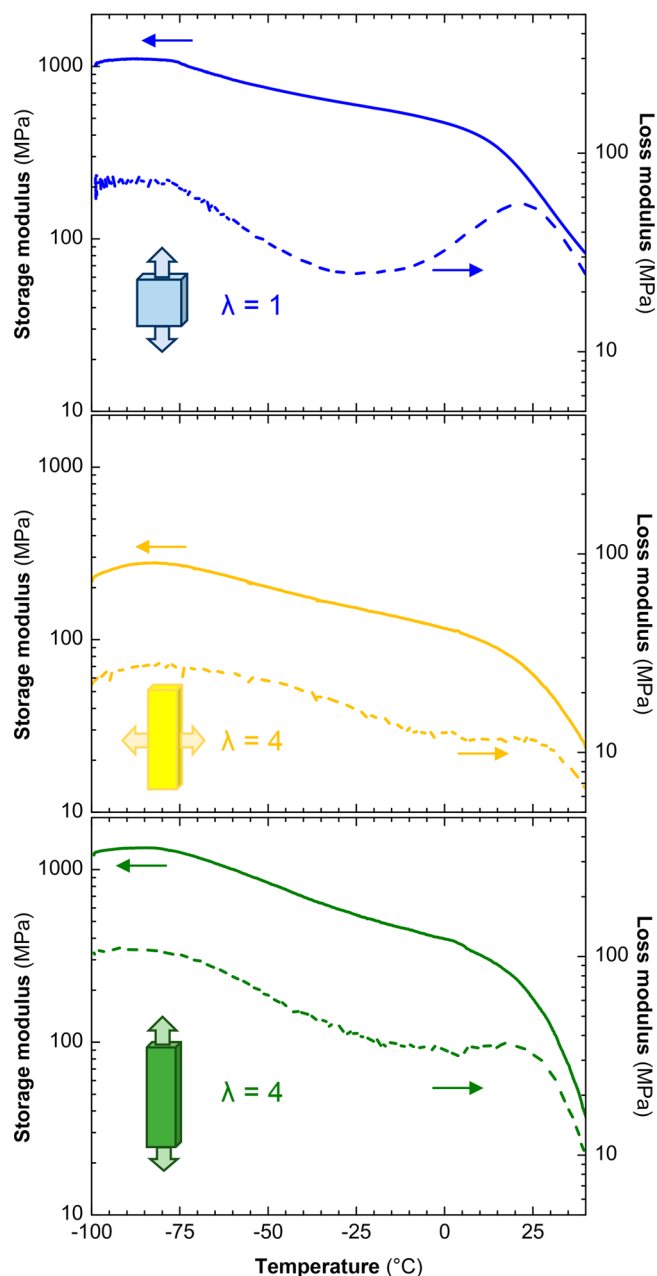


**Figure 3.** Dynamic mechanical analysis (DMA) thermograms of  $\text{Mo}(\text{tfd-COCF}_3)_3$  doped P3HT:  $\lambda = 1$  (blue),  $\lambda \sim 4$  perpendicular to the stretching direction (yellow), and  $\lambda \sim 4$  parallel to the stretching direction (green); Storage and loss modulus,  $E'$  and  $E''$  (solid and dashed lines).

explains why we observe a high electrical conductivity despite the dopant being located only in amorphous domains.

For stretched samples we find increased conductivity both parallel and perpendicular to the drawing direction, with values of  $\sigma_{\parallel} \sim 12.7 \pm 3.3$  S  $\text{cm}^{-1}$  and  $\sigma_{\perp} \sim 1.6 \pm 0.4$  S  $\text{cm}^{-1}$ , respectively, leading to an anisotropy of  $\sigma_{\parallel}/\sigma_{\perp} \sim 8$ . In contrast, the Seebeck coefficient only slightly changes from  $\alpha_0 \sim 138$   $\mu\text{V K}^{-1}$  to  $112$   $\mu\text{V K}^{-1}$  upon drawing, but does not display any anisotropy. As a result, the power factor of  $16$   $\mu\text{W m}^{-1} \text{K}^{-2}$  that we measure along the drawing direction deviates from the empirical trend given by eq 1, leading to a significant gain upon stretching, that is, the power factor is about 5 $\times$  larger than predicted (Figure 4). We also compared our results with

**Table 1.** Draw Ratio  $\lambda$ , Storage and Loss Modulus,  $E'$  and  $E''$ , at 0 °C, Glass Transition Temperature  $T_g$ , and  $\beta$ -Relaxation Temperature  $T_\beta$  from DMA ( $T_g$  and  $T_\beta$  from Peaks of  $E''$ ); Electrical Conductivity  $\sigma$  and Seebeck Coefficient  $\alpha$  at Room Temperature

dopant	$\lambda$ (-)	$T_g$ (°C)	$T_\beta$ (°C)	direction of measurement	$E'$ (GPa)	$\sigma$ (S cm <sup>-1</sup> )	$\alpha$ ( $\mu$ V K <sup>-1</sup> )
none	1	23	-87	isotropic	0.6		
	4	29	-93	$\perp$	0.2		
	4	21	-90	II	1.1		
Mo(tfd-COCF <sub>3</sub> ) <sub>3</sub>	1	21	-91	isotropic	0.5	0.3 $\pm$ 0.1	138 $\pm$ 1
	4	20	-82	$\perp$	0.1	1.6 $\pm$ 0.4	113 $\pm$ 1
	4	17	-90	II	0.4	12.7 $\pm$ 3.3	112 $\pm$ 1

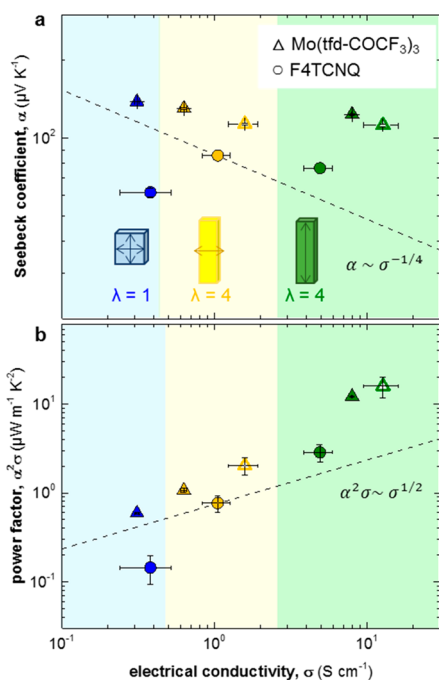


**Figure 4.** (a) Seebeck coefficient  $\alpha$  and (b) power factor  $\alpha^2 \sigma$  as a function of electrical conductivity  $\sigma$  for P3HT doped with Mo(tfd-COCF<sub>3</sub>)<sub>3</sub> (triangles) and F4TCNQ (circles); closed symbols indicate 48 h doping; open symbols indicate 72 h doping; dashed lines show the empirical trends  $\alpha \sim \sigma^{-1/4}$  and  $\alpha^2 \sigma \sim \sigma^{1/2}$ .

F4TCNQ doped films, and find that the conductivity of as-cast P3HT  $\sigma_0 \sim 0.4$  S cm<sup>-1</sup> only increases to  $\sigma_{\parallel} \sim 5$  S cm<sup>-1</sup> for stretched samples, accompanied by a lower Seebeck coefficient of  $\sim 80$   $\mu$ V K<sup>-1</sup>. As a result, the power factor of 3  $\mu$ W m<sup>-1</sup> K<sup>-2</sup> that we measure along the drawing direction does not deviate significantly from the empirical trend given by eq 1.

We constructed a simple model to rationalize the impact of anisotropy on the thermoelectric properties of the doped polymer. The model consists of a two-dimensional resistor network forming a rectangular grid (Figure 5b), where the resistance between sites  $i$  and  $j$  with energies  $E_i$  and  $E_j$ , randomly sampled from an exponential density of states (DOS; disorder = 60 meV),<sup>30,31</sup> is given by

$$R_{ij} = R_0 \times \exp\left(\frac{|E_i - E_F| + |E_j - E_F| + |E_i - E_j|}{2kT}\right) \quad (3)$$

where  $E_F$  is the Fermi level. Using the Einstein relation, the prefactor  $R_0$  can be approximated by

$$R_0 \propto \frac{6kT}{n \times \nu \times \xi^2} \quad (4)$$

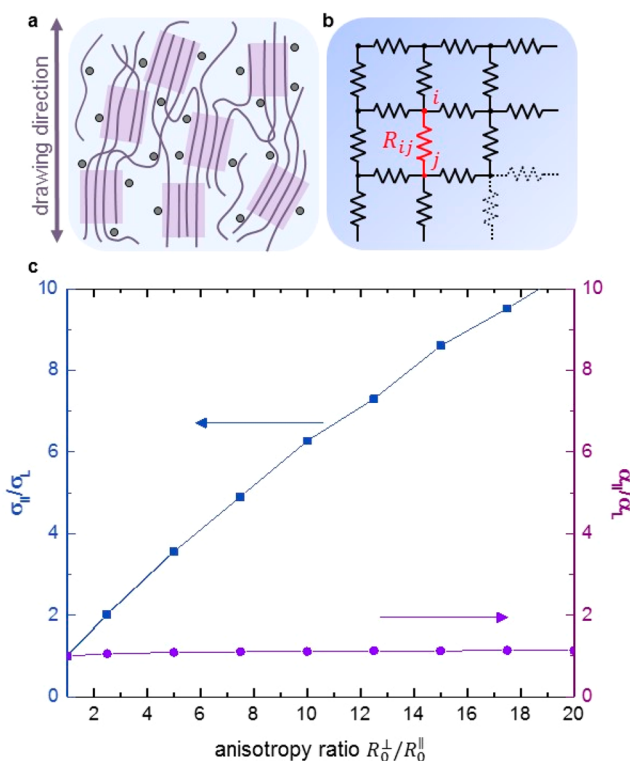


**Figure 5.** (a) Schematic of the nanostructure of tensile drawn P3HT illustrating crystals (purple) within an amorphous matrix (light blue); the dopant Mo(tfd-COCF<sub>3</sub>)<sub>3</sub> (gray circles) is only located in amorphous domains. (b) Two-dimensional resistor network used to simulate the electrical properties of tensile drawn P3HT. Dots indicate hopping sites connected by resistive links. The resistance  $R_{ij}$  depends on the (random) energies  $E_i$  and  $E_j$  of sites  $i$  and  $j$ , as well as the temperature according to the (inverse) hopping rate, as calculated from the Miller-Abrahams expression, as outlined in the Supporting Information. (c) Anisotropy in electrical conductivity  $\sigma_{\parallel}/\sigma_{\perp}$  and Seebeck coefficient  $\alpha_{\parallel}/\alpha_{\perp}$  parallel and perpendicular to the drawing direction (charge carrier concentration  $c = 0.1$ ).

where  $n$  is the total charge concentration,  $\nu$  is the attempt frequency of hopping, which includes the tunneling probability, and  $\xi$  is a characteristic length scale in the direction of the current. Both  $\nu$  and  $\xi$  can differ parallel and perpendicular to the drawing direction, giving rise to two prefactors  $R_0^{\parallel}$  and  $R_0^{\perp}$ . We define an anisotropy ratio as  $R_0^{\perp}/R_0^{\parallel}$  that we vary from  $R_0^{\perp}/R_0^{\parallel} = 1$  for an as-cast and, therefore, isotropic sample, to  $R_0^{\perp}/R_0^{\parallel} \gg 1$  for a highly oriented sample, in which the resistance is lower along the drawing direction due to a higher  $\nu$  and/or  $\xi$ , that is, a higher charge carrier mobility along the drawing direction. Hence, the model assumes that, to a first approximation, stretching the sample affects the relative positions of the hopping sites (i.e., the nanostructure) rather than the site energies.

The anisotropy in conductivity and thermopower are calculated by solving Kirchhoff's laws for the resistor network as detailed in the [Supporting Information](#). We find that the anisotropy in conductivity increases roughly linearly with the anisotropy ratio, reaching a value of  $\sigma_{\parallel}/\sigma_{\perp} \sim 8$  for  $R_0^{\perp}/R_0^{\parallel} \sim 10$  (Figure 5c), while the Seebeck coefficient, in contrast, is only slightly enhanced with increasing anisotropy. Both findings agree with our experimental results (cf. Figure 4a), indicating that the tensile drawing mainly affected the material's nanostructure while preserving the energetics.

We conclude that tensile drawing of the conjugated polymer P3HT creates the opportunity to enhance the thermoelectric power factor when doped with large acceptors such as Mo(tfd-COCF<sub>3</sub>)<sub>3</sub>. The conductivity strongly increases along the drawing direction, whereas the Seebeck coefficient is largely unaffected, leading to a power factor of up to  $16 \mu\text{W m}^{-1} \text{K}^{-2}$ . Doping of oriented samples does not affect the  $T_g \sim 20 \text{ }^{\circ}\text{C}$  and an adequate storage modulus of, for example,  $E_{\parallel}^g \sim 0.2 \text{ GPa}$  is maintained at room temperature, which suggests that tensile drawing is a promising tool for the fabrication of flexible thermoelectric materials.

## ■ ASSOCIATED CONTENT

### Supporting Information

The Supporting Information is available free of charge on the ACS Publications website at DOI: [10.1021/acsmacrolett.8b00820](https://doi.org/10.1021/acsmacrolett.8b00820).

Experimental details, additional characterization, calculation of anisotropy, and supplemental figures (PDF).

## ■ AUTHOR INFORMATION

### Corresponding Author

\*E-mail: [christian.muller@chalmers.se](mailto:christian.muller@chalmers.se).

### ORCID

Stephen Barlow: 0000-0001-9059-9974

Seth R. Marder: 0000-0001-6921-2536

Martijn Kemerink: 0000-0002-7104-7127

Christian Müller: 0000-0001-7859-7909

### Notes

The authors declare no competing financial interest.

## ■ ACKNOWLEDGMENTS

We gratefully acknowledge financial support from the Swedish Research Council through Grant No. 2016-06146, the Knut and Alice Wallenberg Foundation through a Wallenberg Academy Fellowship, and the European Research Council (ERC) under Grant Agreement No. 637624. S.R.M., S.B., and Y.Z. thank the U.S. National Science Foundation for support of this work through the DMREF program, under Award No. DMR-1729737. We thank Katarina Logg and Anders Mårtensson for help with WAXS and SEC measurements.

## ■ REFERENCES

- (1) Lund, A.; van der Velden, N. M.; Persson, N. K.; Hamedi, M. M.; Müller, C. Electrically Conducting Fibres for E-Textiles: An open Playground for Conjugated Polymers and Carbon Nanomaterials. *Mater. Sci. Eng. R Rep.* **2018**, *126*, 1–29.
- (2) Kroon, R.; Mengistie, D. A.; Kiefer, D.; Hynynen, J.; Ryan, J. D.; Yu, L.; Müller, C. Thermoelectric Plastics: From Design to Synthesis, Processing and Structure–Property Relationships. *Chem. Soc. Rev.* **2016**, *45*, 6147–6164.

- (3) Russ, B.; Glauddell, A.; Urban, J. J.; Chabiny, M. L.; Segalman, R. A. Organic Thermoelectric Materials for Energy Harvesting and Temperature Control. *Nat. Rev. Mater.* **2016**, *1*, 16050.
- (4) Glauddell, A. M.; Cochran, J. E.; Patel, S. N.; Chabiny, M. L. Impact of the Doping Method on Conductivity and Thermopower in Semiconducting Polythiophenes. *Adv. Energy Mater.* **2015**, *5*, 1401072.
- (5) Patel, S. N.; Glauddell, A. M.; Peterson, K. A.; Thomas, E. M.; O'Hara, K. A.; Lim, E.; Chabiny, M. L. Morphology Controls the Thermoelectric Power Factor of a Doped Semiconducting Polymer. *Sci. Adv.* **2017**, *3*, e1700434.
- (6) Nogami, Y.; Kaneko, H.; Ishiguro, T.; Takahashi, A.; Tsukamoto, J.; Hosoito, N. On the Metallic States in Highly Conducting Iodine-Doped Polyacetylene. *Solid State Commun.* **1990**, *76*, 583–586.
- (7) Andreatta, A.; Cao, Y.; Chiang, J. C.; Heeger, A. J.; Smith, P. Electrically-Conductive Fibres of Polyaniline Spun from Solutions in Concentrated Sulfuric Acid. *Synth. Met.* **1988**, *26*, 383–389.
- (8) Hiroshige, Y.; Ookawa, M.; Toshima, N. High Thermoelectric Performance of Poly(2,5-dimethoxyphenylenevinylene) and its Derivatives. *Synth. Met.* **2006**, *156*, 1341–1347.
- (9) Motamedi, F.; Ihn, K. J.; Ni, Z.; Srdanov, G.; Wudl, F.; Smith, P. Fibres of Poly(methoxy-2-ethyl-hexyloxy)phenylenevinylene Prepared from the Soluble, Fully Conjugated Polymer. *Polymer* **1992**, *33*, 1102–1104.
- (10) Tokito, S.; Smith, P.; Heeger, A. J. Highly Conductive and Stiff Fibres of Poly(2,5-dimethoxy-p-phenylenevinylene) Prepared from Soluble Precursor Polymer. *Polymer* **1991**, *32*, 464–470.
- (11) Fanous, J.; Schweizer, M.; Schawaller, D.; Buchmeiser, M. R. Crystalline and Conductive Poly(3-hexylthiophene) Fibers. *Macromol. Mater. Eng.* **2012**, *297*, 123–127.
- (12) Moulton, J.; Smith, P. Electrical and Mechanical Properties of Oriented Poly(3-alkylthiophenes) I. Doping-Enhanced Stiffness of Poly(3-octylthiophene). *Synth. Met.* **1991**, *40*, 13–22.
- (13) Tokito, S.; Smith, P.; Heeger, A. J. Mechanical and Electrical Properties of Poly-(2,5-thienylene vinylene) Fibers. *Synth. Met.* **1990**, *36*, 183–194.
- (14) Pukacki, W.; Plochanski, J.; Roth, S. Anisotropy of Thermoelectric Power of Stretch-Oriented New Polyacetylene. *Synth. Met.* **1994**, *62*, 253–256.
- (15) Mateeva, N.; Niculescu, H.; Schlenoff, J.; Testardi, L. R. Correlation of Seebeck Coefficient and Electric Conductivity in Polyaniline and Polypyrrole. *J. Appl. Phys.* **1998**, *83*, 3111–3117.
- (16) Yan, H.; Ohta, T.; Toshima, N. Stretched Polyaniline Films Doped by (±)-10-Camphorsulfonic Acid: Anisotropy and Improvement of Thermoelectric Properties. *Macromol. Mater. Eng.* **2001**, *286*, 139–142.
- (17) Hamidi-Sakr, A.; Biniek, L.; Bantignies, J.-L.; Maurin, D.; Herrmann, L.; Leclerc, N.; Lévêque, P.; Vijayakumar, V.; Zimmermann, N.; Brinkmann, M. A Versatile Method to Fabricate Highly In-Plane Aligned Conducting Polymer Films with Anisotropic Charge Transport and Thermoelectric Properties: The Key Role of Alkyl Side Chain Layers on the Doping Mechanism. *Adv. Funct. Mater.* **2017**, *27*, 1700173.
- (18) Reiser, P.; Müller, L.; Sivanesan, V.; Lovrincic, R.; Barlow, S.; Marder, S. R.; Pucci, A.; Jaegermann, W.; Mankel, E.; Beck, S. Dopant Diffusion in Sequentially Doped Poly(3-hexylthiophene) Studied by Infrared and Photoelectron Spectroscopy. *J. Phys. Chem. C* **2018**, *122*, 14518–14527.
- (19) Koch, F. P. V.; Rivnay, J.; Foster, S.; Müller, C.; Downing, J. M.; Buchaca-Domingo, E.; Westacott, P.; Yu, L.; Yuan, M.; Baklar, M.; Fei, Z.; Luscombe, C.; McLachlan, M. A.; Heeney, M.; Rumbles, G.; Silva, C.; Salleo, A.; Nelson, J.; Smith, P.; Stingelin, N. The Impact of Molecular Weight on Microstructure and Charge Transport in Semicrystalline Polymer Semiconductors-Poly(3-hexylthiophene), a Model Study. *Prog. Polym. Sci.* **2013**, *38*, 1978–1989.
- (20) Duong, D. T.; Wang, C.; Antono, E.; Toney, M. F.; Salleo, A. The Chemical and Structural Origin of Efficient p-Type Doping in P3HT. *Org. Electron.* **2013**, *14*, 1330–1336.
- (21) Hynynen, J.; Kiefer, D.; Yu, L.; Kroon, R.; Munir, R.; Amassian, A.; Kemerink, M.; Müller, C. Enhanced Electrical Conductivity of

Molecularly p-Doped Poly(3-hexylthiophene) through Understanding the Correlation with Solid-State Order. *Macromolecules* **2017**, *50*, 8140–8148.

(22) Méndez, H.; Heimel, G.; Winkler, S.; Frisch, J.; Opitz, A.; Sauer, K.; Wegner, B.; Oehzelt, M.; Röthel, C.; Duhm, S.; Többs, D.; Koch, N.; Salzmann, I. Charge-Transfer Crystallites as Molecular Electrical Dopants. *Nat. Commun.* **2015**, *6*, 8560.

(23) Scholes, D. T.; Hawks, S. A.; Yee, P. Y.; Wu, H.; Lindemuth, J. R.; Tolbert, S. H.; Schwartz, B. J. Overcoming Film Quality Issues for Conjugated Polymers Doped with F4TCNQ by Solution Sequential Processing: Hall Effect, Structural, and Optical Measurements. *J. Phys. Chem. Lett.* **2015**, *6*, 4786–4793.

(24) Müller, C. On the Glass Transition of Polymer Semiconductors and Its Impact on Polymer Solar Cell Stability. *Chem. Mater.* **2015**, *27*, 2740–2754.

(25) Andersson, M. G.; Hynynen, J.; Andersson, M. R.; Hagstrand, P.-O.; Gkourmpis, T.; Müller, C. Additive-Like Amounts of HDPE Prevent Creep of Molten LDPE: Phase-Behavior and Thermo-Mechanical Properties of a Melt-Miscible Blend. *J. Polym. Sci., Part B: Polym. Phys.* **2017**, *55*, 146–156.

(26) Euvrard, J.; Revaux, A.; Nobre, S. S.; Kahn, A.; Vuillaume, D. Toward a Better Understanding of the Doping Mechanism Involved in Mo(tfd-COCF<sub>3</sub>)<sub>3</sub> Doped PBDTTT-c. *J. Appl. Phys.* **2018**, *123*, 225501.

(27) Fujimoto, R.; Yamashita, Y.; Kumagai, S.; Tsurumi, J.; Hinderhofer, A.; Broch, K.; Schreiber, F.; Watanabe, S.; Takeya, J. Molecular Doping in Organic Semiconductors: Fully Solution-Processed, Vacuum-Free Doping with Metal–Organic Complexes in an Orthogonal Solvent. *J. Mater. Chem. C* **2017**, *5*, 12023–12030.

(28) Mohapatra, S. K.; Zhang, Y.; Sandhu, B.; Fonari, M. S.; Timofeeva, T. V.; Marder, S. R.; Barlow, S. Synthesis, Characterization, and Crystal Structures of Molybdenum Complexes of Unsymmetrical Electron-Poor Dithiolene Ligands. *Polyhedron* **2016**, *116*, 88–95.

(29) Qi, Y.; Sajoto, T.; Barlow, S.; Kim, E.-G.; Brédas, J.-L.; Marder, S. R.; Kahn, A. Use of a High Electron-Affinity Molybdenum Dithiolene Complex to p-Dope Hole-Transport Layers. *J. Am. Chem. Soc.* **2009**, *131*, 12530–12531.

(30) Arkhipov, V. I.; Heremans, P.; Emelianova, E. V.; Bäessler, H. Effect of Doping on the Density-of-States Distribution and Carrier Hopping in Disordered Organic Semiconductors. *Phys. Rev. B: Condens. Matter Mater. Phys.* **2005**, *71*, 045214.

(31) Silver, M.; Pautmeier, L.; Bäessler, H. On the Origin of Exponential Band Tails in Amorphous Semiconductors. *Solid State Commun.* **1989**, *72*, 177–180.